scientific reports

Check for updates

OPEN

# Differentiating the thermal effects of land use change and functional intensity dynamics in Beijing

Hongyuan Wei[1], Adu Gong[1]✉, Jinhong Wan[2], Jiaming Zhang[1], Zexin Fu[1] & Mengfei Jiang[1]

**Against the backdrop of global warming, urban heat island (UHI) are driven by both physical land use change and dynamic functional intensity, yet their independent and interactive effects remain poorly understood. This study deconstructs these dual drivers in Beijing. First, we employed the Logistic-Harmonic model and random forest classifier to conduct fine classification of land use changes, and constructed the Urban Function Intensity Index (IDI) based on nighttime light and NDVI time series, analyzing their individual and combined effects on land surface temperature change (ΔLST). Results reveal distinct spatial patterns: the core area is dominated by intensification, while the suburbs are the primary locus of expansion. The thermal response to IDI is spatially and seasonally heterogeneous, with the suburban areas being most sensitive and winter responses being strongest. In suburban areas, high IDI was +0.27°C higher than low IDI in winter, whereas low IDI was -0.24°C higher than high IDI in summer. Critically, the interaction between IDI and LCintensity reveals unique synergistic warming pathways, such as a 'low-IDI + high-intensification' hot spot in the core area driving ΔLST to 0.74°C, and unexpected warming of 0.64°C in suburban areas experiencing 'medium-low IDI + de-urbanization' degradation. Collectively, these findings reveal an evolutionary trajectory of thermal environmental responses across the city's development gradient, providing a new perspective on the "UHI life cycle" in megacities. This study offers a scientific basis for developing targeted, zone-specific thermal regulation strategies.**

**Keywords** Urban heat island (UHI), Land use change, Functional intensity, Spatial heterogeneity, Beijing

The world's urban population is projected to nearly double by 2050, making urbanization one of the most transformative trends of the 21 st century[1]. However, while rapid urbanization provides convenient living, it also leads to the encroachment of construction land on natural surfaces due to urban expansion, causing changes in the underlying surface. In particular, the pattern of impervious surfaces and green spaces in cities, as a key combination of urban land use and land cover, has diametrically opposed effects on surface radiation and energy distribution, directly contributing to the urban heat island effect and having a significant impact on local climate and the thermal regulation of ecological services[2]. The negative impacts of the urban heat island effect extend across multiple social, economic, and ecological dimensions: The increased incidence of adverse interactions between Urban Heat Island and urban pollution islands poses risks to human health and life. Intensified heat waves and air pollution levels increase mortality and disease related to heat stress[3]. The expansion of impervious surfaces and the replacement of natural vegetation by built environments reduce evaporative heat dissipation, thereby intensifying the urban heat island effect. Rapid urbanization puts pressure on urban ecosystems, infrastructure, and energy consumption, exacerbating the growing demand for cooling[4]. Furthermore, elevated urban temperatures can accelerate the photochemical reactions that form ground-level ozone and other pollutants, thus worsening air quality[5]. Rising temperatures can increase the temperature of standing water and impact biodiversity within them[6]. More seriously, the impacts of UHI will be compounded by global warming, which is projected to raise global mean surface temperatures by 1.5–2°C by the end of this century[7]. Consequently, the UHI effect has become a key challenge threatening urban public health, energy security, and ecological sustainability. Against this backdrop, in-depth research on the intensity of urban heat islands driven by diverse land transformations is crucial for developing effective urban climate adaptation plans, mitigating the multiple risks posed by the heat island effect, improving the quality of urban living environments, and promoting sustainable urban development.

[1]Faculty of Geographical Science, Beijing Normal University, Beijing 100875, China. [2]China Institute of Water Resources and Hydropower Research, Beijing 100038, China. ✉email: gad@bnu.edu.cn

While remote sensing has been instrumental in urban studies, current research faces limitations in shifting from a static, structural perspective to a dynamic, functional one. First, remote sensing imagery, as an important recorder of urban surface characteristics, can capture the spatiotemporal dynamics of land use. However, traditional analytical methods often fail to fully exploit the multidimensional information it contains. Studies often focus on a single type of land change, namely physical change or expansion, while overlooking the multifaceted evolution of urban land use[8]. Studies have found that most urban functional area classifications are designed based on the characteristics of land use and data sources. Zou et al.[9] noted that depicting visible forms of surface change (i.e., land use/cover change) benefits from the availability of remote sensing imagery at diverse spatial, temporal, and spectral resolutions. In contrast, characterizing and quantifying implicit forms of surface change, such as land quality, land use efficiency, and land use function, is often difficult to measure directly. Zhu et al.[10] noted that remote sensing data has been widely used to track urban expansion, identify the drivers of urban land demand, and predict future urban growth. Secondly, recent studies have advanced the quantitative understanding of how urban expansion, built environment restructuring, and landscape pattern modifications drive variations in LST across diverse urban contexts. Yu et al.[11] investigated the spatiotemporal dynamics of UHI across 31 major Chinese cities using the local climate zone framework. Their findings indicate significant inter-city variations in UHI intensity from the perspective of urban morphology changes. Urban expansion (UE) and vegetation reduction (VR) were identified as primary contributors to UHI intensification. Both day and night, UE and VR exhibited strong positive correlations with UHI with spatial heterogeneity. Meanwhile, functional transformation of urban areas exerted mixed thermal effects with pronounced nighttime impacts. Li et al.[12] examined the non-linear effects of urban resilience (UR) on surface urban heat island (SUHI) across 349 Chinese cities. They quantified UR from three dimensions: size, density, and morphology. Their findings indicate that UR exerts significant mitigation effects on SUHI with notable spatial heterogeneity, demonstrating stronger cooling effects in high-SUHI cities during daytime and medium-SUHI cities at nighttime, with superior performance in large urban agglomerations. Joshi et al. Joshi and Suneja[13] analyzed changes in LST and Land Use/Land Cover (LULC) composition in Pune City, India, from 2000 to 2023. The results indicate that built-up areas doubled from 40% to 80%, accompanied by a 30% decline in vegetation. These LULC changes led to a significant increase of 16.64°C in LST, confirming that converting natural landscapes to built-up areas is a crucial determinant in exacerbating the SUHI effect. Although SUHI typically refer to the spatial temperature difference between urban and rural areas, understanding their evolution requires long-term temporal analysis. Therefore, this study adopts ΔLST as a proxy indicator to characterize the dynamics of the thermal environment. By analyzing ΔLST, we can directly quantify how specific land transformations have led to the intensification or mitigation of thermal effects during the study period, rather than merely focusing on static urban-rural comparisons. Furthermore, insufficient research on geospatial heterogeneity makes it difficult to accurately identify the dominant factors driving surface temperature changes in different regions, hindering the scientific development of regional climate adaptation strategies and the effective management of the urban heat island effect. Li et al.[14] inferred Beijing's surface temperature from Landsat imagery and, using a combination of geodetectors and a geographically weighted regression model, systematically evaluated the explanatory power of four factors—land cover, topography, socioeconomic status, and meteorology—in contributing to the urban heat island effect and its spatial variation. while studies have successfully identified the spatial heterogeneity of UHI drivers using models like geodetectors, these indicators often rely on static indicators of land cover or socioeconomic status. Consequently, a key knowledge gap remains: how do the dynamic changes in urban functional intensity interact with the physical transformations of land use to shape the spatiotemporal patterns of the urban thermal environment? there is an urgent need to shift from static interpretations of the presence and coverage of impervious surfaces to dynamic quantification and characterization of their functional intensity, in order to better understand the seasonal variations and evolution of thermal environmental characteristics across different functional zones within the city.

To address this gap, this study aims to systematically deconstruct the independent and interactive effects of land use change and urban functional intensity on LST variation, revealing their seasonal evolution and spatial differentiation. To overcome the limitations of traditional research that focuses on the impact of a single land expansion type on LST, we developed an innovative framework that integrates the Logistic-Harmonic model with the random forest algorithm to achieve a fine-grained classification of land use change and construct a novel urban functional intensity index. Nighttime Light (NTL) serves as a proxy for human activity intensity, capturing functional dynamics (e.g., active commercial; dormant residential) that static land cover data cannot. This framework allows for the quantification of the individual and coupled effects of these two factors on LST variation. Furthermore, utilizing long-term nighttime light data, the study analyzes the thermal environmental response gradients across the core, suburban, and exurban zones of Beijing from both seasonal and spatial perspectives. The findings are expected to provide a scientific basis for deepening theoretical understanding of urban thermal environments and for supporting more precise urban spatial planning and thermal regulation strategies.

## Methods

### Data sources and preprocessing

Beijing (116°20′E, 39°56′N), the capital of China, is located in the northern North China Plain and features a warm temperate semi-humid continental monsoon climate. The city's terrain is high in the northwest and low in the southeast, surrounded by mountains on three sides.

For this study, we functionally classified Beijing's 16 districts into three zones based on their official functional designations and development stages (Fig. 1). This study's zoning system considers the city's official functional zoning and recent strategic shifts, providing a functional classification tailored to the research objectives.

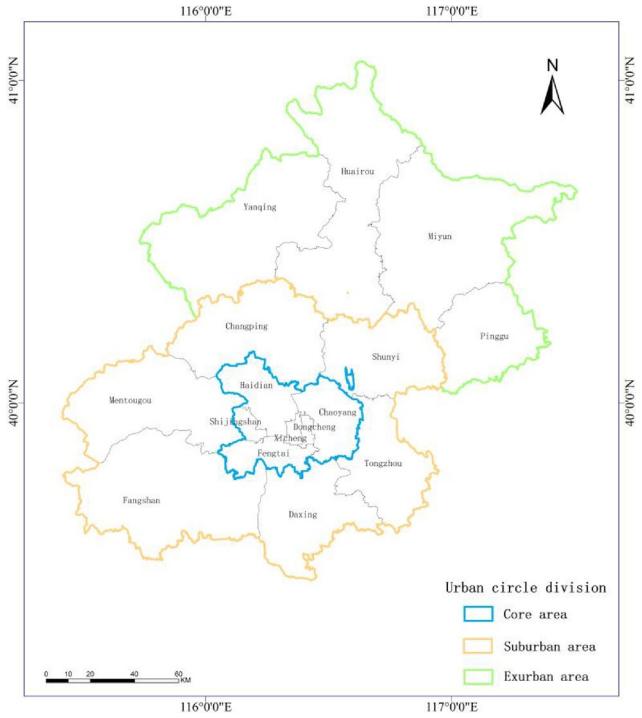


**Fig. 1**. Beijing core area, suburban area, and exurban area circles. The map was generated by the authors using ESRI ArcGIS software (version 10.8, https://www.esri.com/en-us/arcgis/products/arcgis-desktop/overview).

| Data name | Time range | Data type | Resolution | Data source |
|---|---|---|---|---|
| Landsat 8 OLI | 2013 & 2019 | Raster | 30 meters | USGS earth explorer |
| Administrative boundaries of Beijing | / | Vector | / | Resource and environmental science and data center |
| NPP VIIRS nighttime light data | April 2012 to March 2019 | Grid | 500 meters | https://eogdata.mines.edu/products/vnl/ |
| MODIS NDVI (MOD13A1/16 days) | October 2011 to November 2019 | Grid | 500 meters | https://modis.gsfc.nasa.gov/ |
| MCD12Q1 IGBP Data | 2012 to 2019 | Grid | 500 meters | https://modis.gsfc.nasa.gov/ |

**Table 1**. Data and sources.

We combine the "Capital Function Core Area" (Dongcheng District and Xicheng District) and the "Urban Function Expansion Area" (Chaoyang District, Haidian District, Fengtai District, and Shijingshan District) into the core area, representing Beijing's highly mature central urban area. We define the major administrative districts within the "Urban Development New Area" (Tongzhou District, Shunyi District, Changping District, Daxing District, Fangshan District, and Mentougou District) as the suburban area, representing the most actively urbanizing areas. We define the "Ecological Conservation Development Zone" (Pinggu, Huairou Districts, Miyun Districts, and Yanqing Districts) as exurban areas. This classification scheme clearly reflects the spatial gradients of Beijing's different development stages and functional positionin.

Beijing is China's political, cultural, international, and technological innovation center, and is also a first-tier international city and a megacity. According to the Beijing Statistical Yearbook and the Beijing Third National Land Survey Bulletin, its urbanization rate rose slightly from 86.2% to 86.6% between 2012 and 2019. During the same period, the proportion of urban, rural, and industrial and mining land, representing construction land, increased from 18.54% to 19.25%, an increase of 0.71 percentage points, while the proportion of ecological land, such as cultivated land, gardens, woodlands, and grasslands, remained above 73%[15]. This period of steady urban growth, coupled with significant internal transformations, makes Beijing an ideal case for studying the thermal environmental effects of land use evolution under high-intensity human activities.

The data used in this study are shown in (Table 1). Nighttime light data is used to reflect the intensity of human activity, and NDVI data is used to reflect the regulatory capacity of the ecological environment. These two data serve as the basis for constructing the IDI, an index of the dynamic changes in urban functional intensity. Stable sample points of built-up and non-built-up areas were selected from the MCD12Q1 annual land cover data as a training set for subsequent built-up area classification. The Landsat 8 satellite's surface reflectance (SR) product, with its high spatial resolution and spectral diversity, provides an ideal data foundation for accurate LST inversion. To improve data quality, this study implemented cloud and cloud shadow masking, retaining only

images with cloud cover below 50% to minimize cloud interference on the LST inversion. The LST was inverted using the Split Window Algorithm.

Given that the native resolutions of VIIRS and MODIS are 500 m, in order to avoid introducing more errors through interpolation, this study resampled the Landsat LST to 500m. This scale is suitable for the macroscopic gradient analysis of the urban agglomeration in a megacity like Beijing.You et al.[16] conducted a study on the urban heat island effect in the central area of Fuzhou, China, and confirmed that the 500 m grid scale provides the optimal explanatory power for LST and related indicators, because overly large grids would swallow up much of the indicator information, while overly small sample sizes would affect the accuracy of the results.

## Land cover (LC) change classification

*LOGH model*

To capture the nonlinear trends and seasonal fluctuations of urban NTL, we fitted a Logistic-Harmonic (LogH) model to the monthly VIIRS NTL time series on the Google Earth Engine (GEE) platform. First, all VIIRS nighttime light images covering the study area within a specified timeframe were screened on the GEE platform. Two key bands, average radiance and cloud-free number, were extracted from each image. The image collection was then de-banded and stacked image by image. Ultimately, two independent spatiotemporal datasets were constructed: a time series of average radiance (avg_rad) and a time series of cloud-free number (cf_cvg), providing a high-quality data foundation for subsequent model fitting. For the core analysis, this study adapted the nonlinear Logistic-Harmonic (LogH) model proposed by Zheng et al.[8] to fit the monthly NTL time series. This model decouples the long-term evolution of NTL from its intra-annual cyclical variations, modeling it using a logistic term and two harmonic terms, respectively (Equation 1). The logistic term quantifies the nonlinear growth trajectory of light intensity using a sigmoid function. Compared to traditional linear models, this more effectively quantifies the diverse evolutionary patterns of urban development at different stages, thereby more realistically reflecting the inherent laws of urban expansion. Furthermore, the model uses two harmonic terms to eliminate intra-annual seasonal variations in VIIRS data, thereby isolating the true light signal driven by urban land use changes[8].

$$Y_{log}(t) = \frac{\alpha}{1+e^{bt+c}} + d + \sum_{k}^{2}\left[f_k sin(\frac{2\pi kt}{12}) + g_k cos(\frac{2\pi kt}{12})\right] \quad (1)$$

$Y_{log}(t)$ is a mathematical model used to fit time series data. $Y_{log}$ is a function of t (the $t^{th}$ month of observation) and involves the following parameters: a (amplitude factor), b (rate of change), c (time of change), d (initial background radiation value), and $f_k$ and $g_k$ (seasonal amplitude factors). e is the base of the natural logarithm. The number of harmonic terms, k, is set to 2 to account for annual and semiannual seasonal variations based on previous research on the Lomb Scargle periodogram test[8].

*Training a random forest (RF) classifier*

In order to generate a monthly built-up area map, the ideal solution is to obtain high-resolution monthly training samples. However, due to the feasibility and cost of data acquisition, this study adopted an alternative strategy. The core of this strategy is to use the annual MCD12Q1 land cover product to identify "stable pixels" whose land cover types have not changed throughout the study period, and use this to construct a training set. Specifically, for the selected cities, stable pixels that meet the following criteria are screened from MCD12Q1: (1) the land cover type (built-up/non-built-up) of the pixel and its eight adjacent areas remains constant during the study period; (2) to avoid spatial autocorrelation, any two sample pixels are not adjacent. Based on this, 300 built-up and 300 non-built-up stable samples are randomly selected. To ensure the quality of the samples, this study conducted a double verification: 100 built-up and 100 non-built-up pixels were randomly selected from the above samples and visually interpreted and verified with the high-resolution Google Earth images of the same period. If there are more than 5 inaccurate pixels, the batch of samples will be discarded and re-screened. The training features comprise trend parameters extracted from the LogH model, including the Logistic trend term parameters (amplitude factor a, rate of change b, timing of change c, and initial background radiance d), trajectory metrics (radiance values at the initiation, midpoint, and completion of change, as well as change magnitude, duration, and rate), and Harmonic seasonality parameters ($f_k$ and $g_k$ for annual and semiannual variations). These are combined with local features, namely the radiance of the target month and the maximum NDVI within a 12-month window, to construct a multi-dimensional feature space for RF classification. Finally, features derived from the LogH time series modeling of these stable pixels were used to train a Random Forest classifier (Fig. 2). The Overall Accuracy of the classification was 86%.

Classification strategy, based on the aforementioned features, employs the Random Forest algorithm to identify built-up areas separately for the pre-change and post-change stages, thereby discriminating urban land change types (urban concentration, urban expansion, urban degradation, deurbanization, and no change).

Based on the classified land cover status and the NTL intensity trends from the LogH model, urban land use evolution was categorized into the following five types (Table 2):

## Construction of core analytical metrics

*Urban function intensity index (IDI)*

To validate the stratified grouping strategy, the study conducted rigorous evaluations based on both statistical significance and effect size (Table 3). First, the Kruskal-Wallis test results showed that p-values for all three zones were less than 0.001, demonstrating statistically significant differences between the five IDI groups within each stratum, providing preliminary confirmation of the grouping validity.

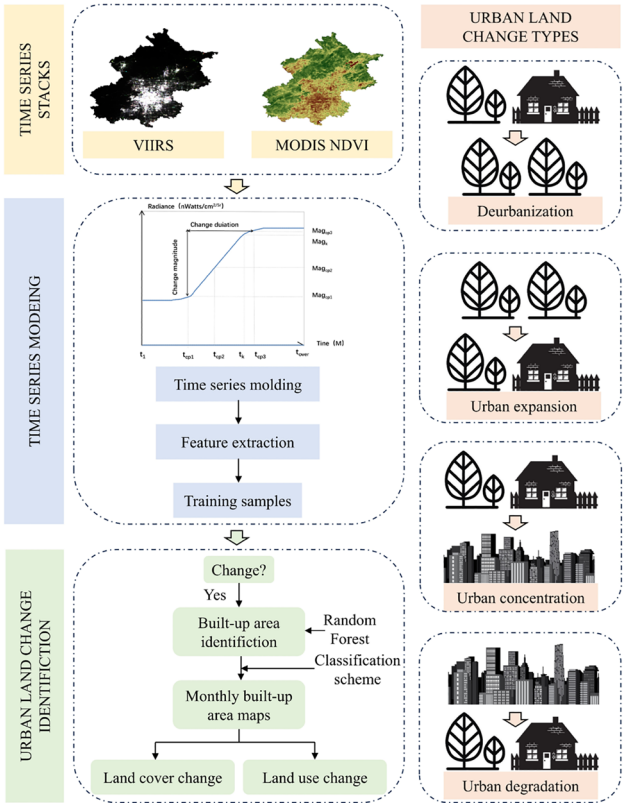


**Fig. 2**. Random forest classification flowchart. This flowchart, including the embedded map thumbnails, was generated by the authors using Microsoft PowerPoint (version 2019, https://www.microsoft.com/) and ESRI ArcGIS software (version 10.8, https://www.esri.com/en-us/arcgis/products/arcgis-desktop/overview).

| Types of urban land change | Before the change | After the change | NTL changes | Describe |
|---|---|---|---|---|
| Urban concentration | Built-up area | Built-up area | Increased strength | Various comprehensive changes occurred in the built-up area, and the NTL intensity increased accordingly. |
| Urban expansion | Non-built-up areas | Built-up area | Increased strength | The biophysical properties of land cover change, and the NTL intensity increases with the change of land cover type. |
| Urban degradation | Built-up area | Built-up area | Weakened strength | The intensity of land use in built-up areas weakened, and the intensity of NTL also weakened. |
| Deurbanization | Built-up area | Non-built-up areas | Weakened strength | With the change of land cover type, the intensity of NTL weakened. |
| No change | Built-up area | Built-up area | No significant fluctuations occurred | During the study period, the area was always built-up or unbuilt-up, and the NTL intensity did not fluctuate significantly. |
| | Non-built-up areas | Non-built-up areas | | |

**Table 2**. Identification of urban land change types.

| Zone | Kruskal_H | Kruskal_p | Difference between high and low IDI groups (°C) | Effect_size |
|---|---|---|---|---|
| Core areas | >500 | <0.001 | 0.03 | Large |
| Suburban areas | >500 | <0.001 | 0.23 | Large |
| Exurban areas | >500 | <0.001 | −0.02 | Large |

**Table 3**. Statistical test results.

To further quantify the differences between high and low IDI groups, Cliff's Delta effect sizes were calculated. The results showed that the differences between high and low IDI groups reached "large effect sizes" across all three strata. Although the effect sizes were consistently high, the absolute ΔLST between the high and low groups exhibited significant spatial variation: the suburban areas exhibited the strongest response, reaching 0.23°C, while the core and exurban areas showed relatively weaker results. Importantly, even in areas with minimal

absolute temperature differences, demonstrates the robustness of our grouping method in capturing a significant, non-random sorting of thermal responses.

First, the urban function intensity index IDI (Equation 2) was constructed using nighttime light and NDVI data to characterize the intensity of human activities.

$$IDI_k = \omega_1 \times (NTL_{norm}) + \omega_2 \times (1 - NDVI_{norm}) \tag{2}$$

$$\mathrm{NTL_{norm}} = \frac{\Delta \mathrm{VIIRS_k}}{\mathrm{Max}\ (\Delta \mathrm{VIIRS})} \tag{3}$$

$$\mathrm{NDVI_{norm}} = \frac{\Delta \mathrm{NDVI_k}}{\mathrm{Max}\ (\Delta \mathrm{NDVI})} \tag{4}$$

Where: k represents different zones, $\omega_1\omega_2$ are weights, uniformly assigned a value of 0.5, April 2012-March 2013 is taken as the starting year, and April 2018-March 2019 is taken as the ending year. The annual average change rates of VIIRS and NDVI by zone, $\Delta\mathrm{VIIRS_k}$ and $\Delta\mathrm{NDVI_k}$, are calculated. $\mathrm{Max}\ (\Delta\mathrm{VIIRS})$ and $\mathrm{Max}\ (\Delta\mathrm{NDVI})$ are the maximum values of the entire study area during the above time periods. These change rates were derived from the long-term trends fitted by the LogH model to ensure robustness.

Then, the Z-score of the entire study area is normalized (Equation 5).

$$\mathrm{IDI_z} = \frac{(\mathrm{IDI} - \mu_{\mathrm{IDI}})}{\sigma_{\mathrm{IDI}}} \tag{5}$$

Where μ is the mean of the dataset, and σ is the standard deviation.

Finally, based on the spatial distribution of $IDI_z$ in the study area, we used the 20th, 40th, 60th, and 80th percentiles as classification points and assigned the following group labels: Low, Medium-Low, Medium, Medium-High, and High, respectively.

*Land change intensity ($LC_{intensity}$)*

To quantify the diverse impacts of different land use transition patterns, we developed a continuous metric named $\mathrm{LC_{intensity}}$. Based on expert knowledge, this approach is based on the premise that different modes of urban evolution, such as expansion versus internal intensification, have distinct thermal environmental consequences.

This study constructs a continuous $LC_{intensity}$ metric with a range of [−1.0, 1.0] to accurately characterize the intensity and directional properties of land-use change (LC). The indicator design is based on the physical connotations of the five LC categories, reflecting the intensity of change through absolute values and using positive and negative signs to indicate the direction of change (positive signifies intensification or urban expansion, negative signifies degradation or de-urbanization).

The specific value assignment system is as follows: intensification (high-intensity development) +1.0, urban expansion (medium-to-high-intensity development) +0.7, baseline (no change) 0.0, urban degradation (functional decline) −0.3 and de-urbanization (functional extinction) −0.5. This ranked assignment reflects the varying intensity of development and its expected environmental impact.

## Statistical analysis framework

*Gradient effect analysis*

To rule out multicollinearity between IDI and LC, we calculated the Variance Inflation Factor (VIF). All VIF values were less than 10, indicating no severe collinearity.

All thermal environmental responses were quantified using ΔLST, defined as the mean land surface temperature at the end year minus the mean land surface temperature at the start year. To analyze the urban gradient effect, we first classified all grid cells into five levels based on their standardized IDI. We then calculated the mean ΔLST and its 95% confidence interval for each of the five IDI levels across three temporal scales: annual, winter, and summer(Equation 6).

To quantify the overall magnitude of the gradient effect, we defined the temperature gradient (Δ_grad) as the difference in mean ΔLST between the highest (High) and lowest (Low) IDI groups.

$$\Delta_{grad} = mean\,(\Delta LST_{High}) - mean\,(\Delta LST_{Low}) \tag{6}$$

Where: $\Delta_{\mathrm{grad\_}}$ is the surface temperature gradient between the high and low IDI areas, $mean(\Delta\mathrm{LST_{High}})$ is the arithmetic mean of the surface temperature change before and after the high IDI period, and $mean(\Delta\mathrm{LST_{Low}})$ is the arithmetic mean of the surface temperature change before and after the low IDI period.

*Land change intensity effect*

To investigate the impact of different types of land change on land surface temperature, land change data for each sphere were assigned a value based on the continuous intensity index ($\mathrm{LC_{intensity}}$) defined in Section "Land change intensity ()". A two-dimensional kernel density estimation (2D KDE) was used to visualize the two-dimensional relationship between land change intensity and ΔLST. Since a land change type (LC) value of 0 represents a baseline area with no change, this study focuses on the thermal effects of significant changes such as urban intensification, expansion, degradation, and deurbanization. Therefore, the visualization deemphasizes the response characteristics of areas experiencing changes, highlighting the response characteristics of areas experiencing changes. Within the 2D-KDE plot, the median ΔLST for the main change types was annotated to highlight their central tendency.

*Interaction effect analysis*

To systematically explore the interactive impact of IDI and LC on LST, we conducted a quantitative analysis based on their combined groupings. We classified $\mathrm{LC}_{\mathrm{intensity}}$ into five quintile groups (L1 to L5), analogous to the IDI groups (Q1 to Q5). This created a 5×5 matrix representing all possible combinations of IDI and $LC_{intensity}$ levels. We then calculated the mean ΔLST for the grid cells within each combination bin.

The results were visualized using interactive heat maps for the annual, winter, and summer periods. These heat maps clearly demonstrate the significant impact of high-intensity combinations (such as high IDI and high-intensity urban development) on the urban heat island effect, providing a scientific basis for in-depth analysis of its spatial heterogeneity and its formation mechanisms.

## Results

### Spatial pattern of land use change

The classification results of the VIIRS monthly nighttime light time series modeling for Beijing from April 2012 to March 2019 are divided into two parts: one showing the distribution of land cover type changes (urban expansion and de-urbanization) and the other showing the distribution of built-up area changes (urban intensification, urban degradation, and no change). The reclassification results are shown in the figure. As shown in Fig. 3, urban expansion and de-urbanization are mainly distributed in the connecting areas between Beijing's core area and suburban areas, radiating outward. As shown in Fig. 4, urban intensification and urban degradation are mainly occurring in Beijing's core area.

Statistical analysis reveals distinct patterns of land use change across the three zones (Table 4). The core area is dominated by intensification, which accounts for 25.40% of its total area. After years of development, the core area has developed a mature urban fabric, and the contradiction between land scarcity and urban development needs is becoming increasingly prominent. Given limited land resources, intensive development has become an inevitable choice for optimizing the spatial structure and improving land use efficiency in the core area.

The suburban area serves as the main frontier of urban growth, exhibiting the highest proportion of urban expansion (1.37%). This is closely related to the stage-by-stage characteristics of urban development. With the functional saturation and industrial upgrading of the core area, suburban areas naturally become important vehicles for absorbing the functional spillover from the core. By absorbing industries and population relocated from the core area, suburban areas effectively alleviate development pressure in the core area while also injecting new momentum into their own development, forming a spatial pattern of complementary and coordinated development with the core area.

In the outer suburbs, Beijing's ecological conservation area, urban concentration accounts for only 0.79%, while urban expansion accounts for 0.53%, reflecting the clarity of the regional functional positioning. Beijing strictly implements urban planning and land use control policies, protects forests, cultivated land, water conservation areas, and agricultural, forestry, animal husbandry, and fishery resources. It strictly controls development and construction in ecological conservation areas, strictly enforces the new industry access system, and adheres to ecological protection red lines to ensure that regional ecological functions are not damaged. This

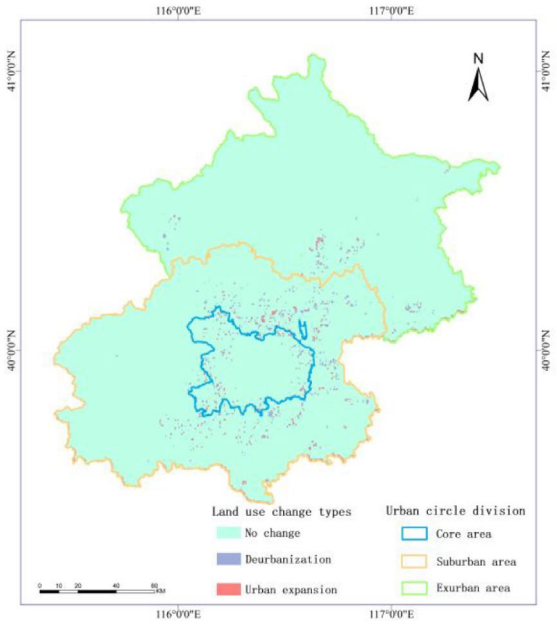


**Fig. 3**. Reclassification of land cover type changes. The map was generated by the authors using ESRI ArcGIS software (version 10.8, https://www.esri.com/en-us/arcgis/products/arcgis-desktop/overview).

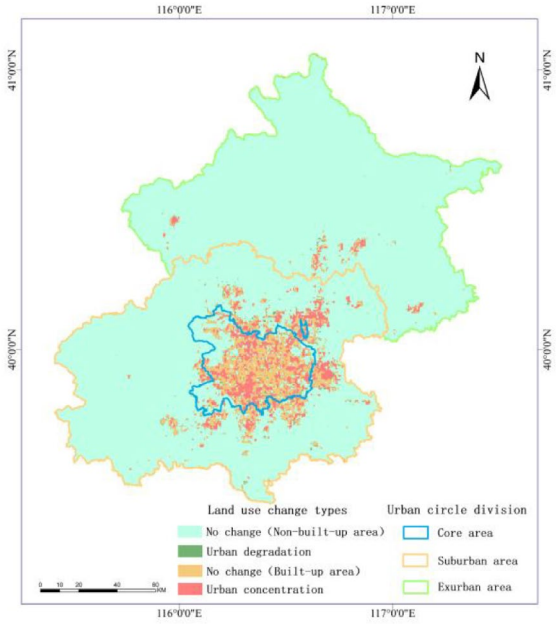


**Fig. 4**. Reclassification of built-up area changes. The map was generated by the authors using ESRI ArcGIS software (version 10.8, https://www.esri.com/en-us/arcgis/products/arcgis-desktop/overview).

| Circle | Intensification | Urban degradation | Urban expansion | Deurbanization |
|---|---|---|---|---|
| Core | 25.40% | 2.06% | 1.24% | 3.02% |
| Suburban | 4.01% | 0.64% | 1.37% | 1.92% |
| Exurban | 0.79% | 0.14% | 0.53% | 0.54% |

**Table 4**. Statistics of land use change proportions.

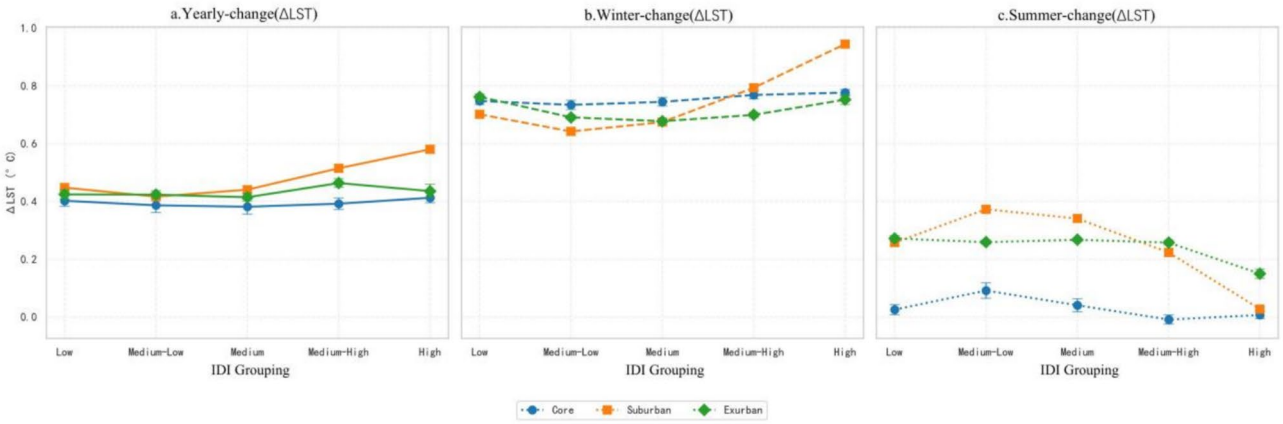


**Fig. 5**. IDI gradient response (a year-round, b winter, c summer).

low-intensity development model not only meets the city's basic needs for ecological security, but also provides ecological guarantees for its sustainable development.

## Thermal response to the IDI gradient

The IDI gradient effect exhibits significant spatial heterogeneity across the three zones (Fig. 5). Three main patterns were observed based on the annual ΔLST response (Fig. 5a). the suburban areas exhibit the most pronounced gradient effect. However, the difference between high and low IDI groups in the suburban areas

is most pronounced, with ΔLST values of 0.58±0.01°C for the high IDI group and 0.45±0.01°C for the low IDI group. The difference between the high and low IDI groups is nearly 0.13°C. Furthermore, looking at the full year trend in the suburban areas, ΔLST begins to rise in the mid-high and high IDI groups, exceeding the ΔLST of the low IDI group by 0.05°C and 0.13°C, respectively. This indicates that the higher intensity of human activity in the suburban areas has a more significant warming effect on surface temperature.

A vertical comparison across the zones reveals that the suburban and exurban areas consistently have higher overall ΔLST values than the core area. This suggests that the most significant warming during the study period occurred outside the city center. Notably, the suburban areas generally show the highest sensitivity to increasing IDI, as indicated by the steeper slope of their response curve, particularly at higher IDI levels.

The IDI gradient effect exhibits strong seasonal differentiation (Fig. 5b, 5c). The effect is pronounced in winter, particularly in the suburban areas, where high-IDI groups exhibit +0.27°C higher LST than low-IDI counterparts. In contrast, the response in the core and exurban areas remains muted during winter. This suggests that human activities in the suburbs have a significant spatial sensitivity to the warming effect of LST. During summer, significant differences in temperature between the high and low IDI groups exist between the suburban and exurban areas, at −0.24°C and −0.12°C, respectively. The difference is more pronounced in the suburban areas, while the difference between the core and exurban areas is insignificant. Notably, the three-sphere gradient response exhibits a unique pattern in summer: the influence of the suburban and exurban areas on land surface temperature decreases under high IDI conditions, indicating seasonal differentiation in the thermal environment regulation mechanism.

Comparative analysis of the IDI-LST response curves for the entire year, winter, and summer revealed significantly greater fluctuations in the suburban area's IDI-LST response curve than in the core area and exurban areas, again demonstrating that human activities in the suburbs have the most significant impact on surface temperature.

Overall, the seasonal comparison confirms that the thermal environment's sensitivity to human activity intensity (as represented by IDI) is significantly stronger in winter than in summer. T This finding is consistent with the known characteristics of the urban heat island effect, which is often more pronounced in winter due to factors like lower solar angles and increased anthropogenic heat from heating.

## Spatial heterogeneity of land change intensity effects

The relationship between land change intensity ($LC_{intensity}$) and ΔLST is visualized using two-dimensional kernel density estimation (2D-KDE) plots for each zone (Fig. 6).The horizontal axis represents land change intensity, and the vertical axis represents ΔLST. ΔLST values are primarily distributed within the range of −1.0°C to +1.5°C. The color gradient reflects the concentration of data points (darker areas indicate high density), and the red dashed line represents the median.

The core area exhibits a bimodal distribution. first, abnormally high temperature samples (ΔLST>0.8°C, accounting for 32%) are found in the de-urbanized area ($LC_{intensity}$=−0.5); second, a concentrated area of temperature variation is formed in the $LC_{intensity}$ range of 0.5–1.0.5.0. The median ΔLST in the intensive development area ($LC_{intensity}$=1.0) reaches 0.47°C, which is significantly higher than the 0.41°C of the urban expansion type ($LC_{intensity}$=0.7) and the 0.36°C of the entire core area, indicating that intensive development is the dominant factor in the increase in surface temperature in the core area.

The suburban area exhibits a distinct oblique zonal distribution, with a peak ΔLST of 0.84±0.13°C occurring in the $LC_{intensity}$ range of −0.3 to −0.5, the highest value in the entire sample and significantly higher than the 0.45±0.03°C (t=3.05, p=0.003) observed in the moderately developed areas of the same region. The median ΔLST in this region is 0.54°C, confirming that urban degradation and deurbanization are the primary driving mechanisms of LST change in the suburban area.

The exurban areas also exhibit a bimodal distribution: First, high-density clusters form in the $LC_{intensity}$ range of 0.5–1.0.5.0. The median ΔLST in the urban expansion area ($LC_{intensity}$ = 0.7) reaches 0.88°C, significantly higher than the 0.22°C in the unchanged area and higher than the 0.62°C median ΔLST for the

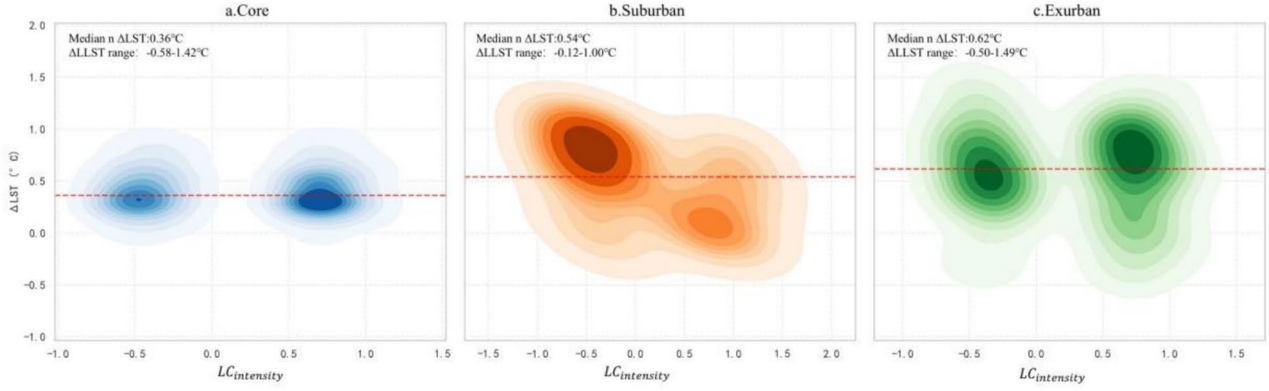


**Fig. 6**. Relationship between land change intensity and ΔLST (a core area, b suburban area, c exurban area).

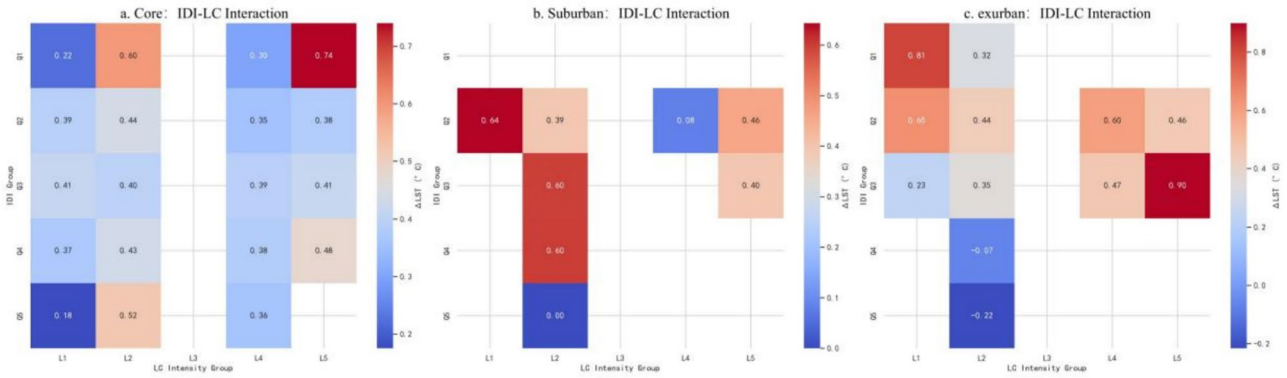


**Fig. 7**. IDI-LC interaction effect diagram (a core area, b suburban area, c exurban area).

| Circle | Hot combination | ΔLST(°C) | Baseline group | Statistical test results |
|---|---|---|---|---|
| Core areas | Q1L5 (low IDI + intensive) | 0.74 | Q5L1 (high IDI + de-urbanization) | *** |
| Suburban areas | Q2L1 (medium-low IDI + de-urbanization) | 0.64 | Q5L2 (high IDI + urban degradation) | ** |
| | Q3L2/Q4L2 (medium/medium-high IDI + urban degradation) | 0.60 | | |
| Exurban areas | Q3L5 (Medium IDI + Intensive) | 0.90 | Q5L2 (high IDI + urban degradation) | *** |
| | Q1L1 (low IDI + deurbanization) | 0.81 | | |

**Table 5**. Statistics of the IDI-LC interaction effect strength. Note:*p<0.05, **p<0.01, ***p<0.001.

entire exurban area. Second, a slight cooling trend (ΔLST = −0.12 ± 0.08°C) is observed in the deurbanized area. Statistical results indicate that urban expansion is the dominant factor in exurban surface temperature changes.

A cross-zone comparison reveals that urban expansion consistently leads to ΔLST values above the respective zone's median, particularly in the exurban areas. Conversely, urban degradation generally corresponds to ΔLST values below the median. This confirms that while expansion is the primary driver of warming in the exurbs, intensification is the dominant warming factor in the core area.

### Interaction effects of IDI and Land Change Intensity

To identify the interactive effects of IDI and $LC_{intensity}$, we analyzed the mean ΔLST for each of the 25 combined groups (IDI quintiles Q1-Q5 vs. $LC_{intensity}$ quintiles L1-L5). The results are visualized in heat maps (Fig. 7), and the statistically significant "hot spot" combinations for each zone are summarized in Table 5. A "hot spot" is defined as a combination whose mean ΔLST is significantly higher than that of a designated baseline group. Each zone reveals a unique interaction pattern.

The core area analysis showed that the ΔLST of the Q1 and L5 combination (low IDI + intensification) reached 0.74°C, which was significantly higher than that of the baseline group Q5 and L1 (high IDI + deurbanization) (0.18°C). The incremental interaction effect reached 0.56°C (t=3.89, p<0.001), indicating that there was a significant "low IDI-high development intensity" synergistic warming effect in the core area.

Suburban areas exhibited multiple significant interactions: the ΔLST for Q2 and L1 (medium-low IDI + deurbanization) was 0.64°C, while the ΔLST for Q3 and L2 (medium IDI + urban degradation) and Q4 and L2 (medium-high IDI + urban degradation) combinations were both 0.60°C. If the Q5 and L2 group (high IDI + urban degradation), with an effect value of 0.00 in the figure, was used as a control group, the warming effects of all three groups were significant. This confirms that the synergistic patterns of "medium-low IDI + deurbanization" and "medium/medium-high IDI + urban degradation" in suburban areas have a significant warming impact on the thermal environment.

Two strong interaction combinations were identified in the exurban areas: Q3 and L5 (medium IDI + intensification) with a ΔLST of 0.90°C, and Q1 and L1 (low IDI + deurbanization) with a ΔLST of 0.81°C. Both were significantly higher than the baseline group Q5 and L2 (high IDI + urban degradation) (−0.22°C), revealing that the exurban areas have two different strong synergistic warming pathways: 'medium IDI-intensive development' and 'low IDI-deurbanization', and that they interact significantly with the medium and low IDI levels (Q1, Q2, Q3).

## Discussion

### Unlocking new perspectives on the complexity of urban thermal environments

Urban land-use change goes far beyond the physical expansion of built-up areas. It also involves a variety of complex phenomena, including spatial conversions of land-use types, dynamic adjustments in land-use intensity, and the evolution of urban functional zones[17]. To this end, this study adopted a novel methodological approach:

fitting the VIIRS monthly NTL data with a logistic-harmonic model, combined with the advantages of random forest feature recognition and classification, to more accurately reflect the diversity and dynamics of urban land-use change, rather than simply providing information on "presence or absence" or "expansion"[8].

Furthermore, to quantitatively compare the impacts of different land-use transition patterns, this study constructed a continuous $LC_{intensity}$ metric to convert categorical variables into continuous variables. This approach of quantifying and grading the environmental impacts of different land-use transition patterns has been widely applied in fields such as ecological risk assessment and ecosystem service valuation[18,19], and has proven to be an effective approach for understanding the complex effects of urbanization. Recent studies on the urban thermal environment have further demonstrated that different urban development models, such as urban expansion and renewal and intensification within built-up areas, have significantly different impacts on surface temperature[20,21], which provides direct empirical support for the assignment system of this study.

On this basis, to effectively address spatial autocorrelation and overcome the limitations of single-site research on land change in suburban and exurban areas, this study innovatively constructed a hierarchical and grouped statistical framework, achieving a refined representation of urban spatial structure. By applying Z-score standardization and quintile grouping to the city-wide IDI, cross-sector comparisons were ensured to be scientific and consistent.

Finally, our hierarchical grouping framework, based on a city-wide standardized IDI, ensures robust and comparable analysis across different urban zones. This integrated approach—from fine-grained classification to continuous quantification and then to robust hierarchical statistics—provides a powerful and scalable toolkit for disentangling the complex human-environment interactions within urban systems, including annual, winter, and summer averages.

## Differentiated thermal response mechanisms across urban zones

Our findings reveal that the driving mechanisms of the thermal environment vary significantly across different urban zones, reflecting their distinct development stages.

In the exurban areas, high-intensity development (i.e., urban expansion) was the dominant driver of warming. The underlying mechanism is that development is accompanied by large-scale vegetation removal. Vegetation, a natural "temperature regulator," achieves its cooling function primarily through two pathways: first, through transpiration, it consumes significant amounts of solar radiation, reducing the amount converted into sensible heat (i.e., temperature increase); and second, through canopy shading, it directly blocks solar radiation from heating the surface[22]. Therefore, the removal of vegetation during expansion directly weakens this natural temperature regulation, leading to significant surface warming.

In contrast, the core area exhibited a "saturation effect," where intensive development was the primary driver of warming. This phenomenon is highly consistent with findings from a study in the São Paulo Center, Brazil. Morais et al.[23] pointed out that the "urban canyon" structure formed by high-rise buildings and narrow streets significantly hinders the dissipation of heat to the outside world, creating a heat "trapping" effect, which significantly increases surface and air temperatures. Qiao et al.[24] used MODIS surface temperature data from 2003 to 2017 to explore the spatiotemporal characteristics and evolution of Beijing's surface thermal landscape, and concluded that the high temperatures in the city center are primarily due to the expansion of impervious surfaces and anthropogenic heat emissions. Therefore, urban planning should focus on optimizing building layout and street design, controlling the ratio of building height to street width, and increasing cooling sources such as green space and water bodies to mitigate the urban heat island effect.

Perhaps the most noteworthy finding, as reported in Section "Thermal response to the IDI gradient", is the cool island effect observed in summer, where high-IDI areas showed lower ΔLST than low-IDI areas. A plausible explanation for this counterintuitive phenomenon involves multiple interacting factors, with a similar case observed in Tehran. Aghazadeh et al.[25] revealed a thermal paradox: while green spaces were the coolest zones in 2000, built-up areas had become cooler by 2020, with LST decreasing by 2.71 °C compared to a negligible increase of 0.12 °C in green spaces. This inversion is primarily attributed to morphology-driven cooling, where increased building height and density reduced the sky-view factor and enhanced shading. Additionally, increased albedo and improved vegetation health were identified as contributing factors.

In the context of Beijing, three-dimensional greening and policy-driven vegetation cooling play a pivotal role. High-IDI areas, such as central business districts and newly built high-density communities, are often where advanced green infrastructure has been most heavily deployed. Zhang et al.[6] noted that these areas are increasingly incorporating advanced greening strategies such as green roofs and vertical gardens, with reported surface temperature reductions of up to 15 °C relative to conventional roofs. To address the scarcity of urban open space, Beijing launched its urban vertical greening program in 2011. By 2017, over one million square meters of building roofs had been renovated, with plans to add 100,000 to 120,000 square meters of green roofs annually by 2020. More significantly, Beijing has implemented large-scale ecological projects. Since September 2012, Beijing has accelerated afforestation in the plain area to build urban forests. Two rounds of the "Million Mu Afforestation" project were carried out from 2012 to 2015 and 2018 to 2022, adding over 1.9 million mu of forest to Beijing's plains and creating large-scale forest landscapes. Expert assessments confirm a marked climate regulation effect Forestry and Parks Bureau[26]. In terms of policy, the "Implementation Plan for Promoting Ecological Protection and Green Development in the Ecological Conservation Zone in the New Era" stipulates that by 2027, the area of ecological protection red lines should remain at no less than 27.5% of the city's total area, and the area of ecological control zones should strive to reach 75%. The overall forest coverage of Mentougou, Pinggu, Huairou, Miyun, and Yanqing districts will be maintained above 66%, with further enhancements in forest stock volume and ecological carbon sink capacity[27].

Furthermore, building shading, thermal inertia differences, and high-albedo material applications provide additional cooling contributions. High-IDI areas feature extremely tall and dense buildings. In summer, high-

rise buildings create extensive shadows among themselves. Satellites typically transit around 10:30 AM, at which time the surface temperature in the shadows of high-rises is far lower than that of sunlit suburban low-rise buildings or bare ground. Liu et al.[28] support this mechanism, finding that alleys with high canopy coverage and broad streets equipped with road-center hedges demonstrate superior cooling capabilities, with cooling effects of 23.56% and 18.81%, respectively. They suggest that moderately elevated building heights along wide streets could maximize cooling benefits through building shadows. Meanwhile, differences in thermal inertia of surface materials are notable: high-density core areas composed of concrete and steel have high thermal inertia and heat up slowly, whereas suburbs often consist of lightweight materials (e.g., color steel plate roofs or dry bare soil) with low thermal inertia, which heat up rapidly under morning sunlight. Su et al.[29] also corroborated that suburbs, with more open land and bare ground, respond faster to solar radiation in the early morning, leading to faster LST increase,conversely, urban areas with extensive building shading and high impervious surface coverage exhibit slower LST warming. Additionally, the application of high-albedo materials contributes to cooling. Vujovic et al.[30] highlighted that an albedo increase of 0.25 can lower pavement surface temperature by 10 °C, while replacing asphalt with reflective concrete can reduce surface air temperature by 0.20–0.40°C.

It is worth noting that the identified degradation and de-urbanization in the suburbs are primarily driven by Beijing's policy to relieve non-capital functions, not by economic recession. The period from 2012 to 2019 was crucial for Beijing's "Shujie Zhengzhi Cujin Tisheng" campaign. Beijing became the first city in China to propose "quantity-reduced development," focusing on high-quality growth in high-end, precision industries rather than extensive expansion. Since 2017, Beijing has demolished over 200 million square meters of illegal construction, reducing urban and rural construction land by 110 square kilometers[31]. Post-demolition land is often bare soil or construction waste with low heat capacity, heating up quickly and leading to high ΔLST peaks.

In conclusion, the shading provided by tall buildings and tree canopies, combined with high-albedo materials and three-dimensional greening, substantially lowers surface temperatures by reducing solar radiation absorption and increasing evapotranspiration. High thermal inertia materials further retard surface heating, collectively resulting in the lower surface temperatures observed in high-IDI areas during summer. However, uncertainties remain. Li et al.[32] found that the urbanization-induced warming effect was significantly correlated with impervious surface changes and multi-year average precipitation, whereas its relationships with urban population and GDP were not significant. This indicates that physical land surface changes and climatic background offer stronger explanatory power than socioeconomic indicators. Additionally, unconsidered factors such as cloud cover and aerosol concentration, as well as spatial scale dependency, constitute significant sources of uncertainty.

The results of this study reveal Beijing's unique "Core areas saturation-Suburban areas disturbance" thermal structure, which differs significantly from the traditional urban heat island patterns observed in other mega-cities in China. Xu et al.[33] found that in Shanghai, the Urban Heat Island Intensity exhibits a descending trend from the inner ring to the outer ring. In contrast, driven by Beijing's "quantity-reduced development" policy, measures such as large-scale plain afforestation, three-dimensional greening (green roofs and vertical gardens), building morphological shading, and high-albedo material application have effectively lowered the LST in high-IDI Suburban areas, creating a daytime cool island effect in summer. This finding indicates that proactive ecological regulation and morphological optimization can reshape the urban thermal landscape, providing new empirical evidence for understanding the anthropogenic regulation mechanisms of the thermal environment in mega-cities.

## Conclusion

This study investigated the dual impacts of urban functional intensity dynamics and land use transitions on the thermal environment of Beijing from 2012 to 2019. By developing a novel analytical framework that integrates time series modeling, a continuous characterization of land change, and a unified hierarchical grouping strategy, we systematically deconstructed the independent and interactive effects of these two drivers. Our findings provide a new perspective on the spatially and seasonally differentiated mechanisms of UHI formation in a megacity, offering scientific support for sustainable urban planning and practices.

The main conclusions are as follows:

(1) Spatial differentiation: Land use change exhibits significant spatial differentiation in driving factors of land surface temperature. The core areas are dominated by intensification as the primary driver; the exurban areas, serving as ecological conservation zones, are mainly driven by urban expansion; the suburban areas become the dual carrier of urban expansion and functional decentralization, where urban degradation and de-urbanization phenomena emerge as key variables regulating surface temperature changes.
(2) Seasonal heterogeneity: The thermal response of urban functional intensity to land surface temperature shows marked seasonal heterogeneity. In summer, high-IDI suburban areas exhibit a counterintuitive cooling trend, with the three-zonal gradient response displaying a special pattern. This cool island effect stems from the combined effects of eco-physical interventions (three-dimensional greening, urban morphological optimization, high-albedo material application, and thermal inertia management) and policy regulations (quantity-reduced development, plain afforestation, and ecological conservation and green development in conservation zones), confirming that proactive anthropogenic regulation can effectively reshape urban thermal patterns. Winter returns to the conventional urban heat island mode, with clear seasonal boundary conditions.
(3) Synergistic pathways: The interaction between functional intensity and land change($LC_{intensity}$) reveals unique synergistic pathways. The core areas display a "low IDI–high development intensity" warming pattern; the suburban areas identify "medium IDI–de-urbanization" and "medium IDI–urban degradation"

disturbance patterns; the exurban areas exhibit a dual "urban expansion–de-urbanization" pathway, reflecting the dynamic balance between ecological conservation and urban development.

This study has limitations that suggest avenues for future research. First, the study period ends in 2019. Extending the time series to include the post-pandemic period would provide valuable insights into how major public health events affect urban functional intensity and thermal patterns. Second, our analysis is based on land surface temperature. Integrating atmospheric data, for instance by using models like the Weather Research & Forecasting model, could provide a more comprehensive, three-dimensional understanding of the urban thermal environment[34]. Third, our $LC_{intensity}$ metric is based on a ranked assignment,future work could explore driven methods to derive these weights.

In conclusion, this study reveals a clear evolutionary trajectory of the urban thermal environmental response across Beijing's developmental gradient. The response evolves from a sensitive, IDI-driven stage in the exurbs, to a complex and disordered stage in the suburbs, and finally to a saturated, less responsive stage in the core area. This finding provides strong empirical support for a "UHI life cycle theory" in megacities and offers a new framework for understanding their thermal evolution. The insights from Beijing's three zones can serve as a valuable reference for cities at different development stages, aiding in the formulation of more precise and effective UHI mitigation strategies.

## Data availability

All data generated or analysed during this study are included in this published article.

Received: 13 January 2026; Accepted: 16 March 2026
Published online: 29 March 2026

## References

1. United Nations Conference on Housing and Sustainable Urban Development (Habitat III). *New Urban Agenda* (United Nations, 2016).
2. Kuang, W. H. Advance and future prospects of urban land use/cover change and ecological regulation of thermal environment. *Sci. Geogr. Sin.* **38**(10), 1643–1652 (2018).
3. Cichowicz, R. & Bochenek, D. A. Assessing the effects of urban heat islands and air pollution on human quality of life. *Anthropocene* **46**, 100433 (2024).
4. Tehrani, A. A. et al. Data-driven approach to estimate urban heat island impacts on building energy consumption. *Energy* **316**, 134508 (2025).
5. Jinsil, P. et al. Efficient plant types and coverage rates for optimal green roof to reduce urban heat island effect. *Sustainability.* **14**(4), 2146 (2022).
6. Zhang, L., Fukuda, H. & Liu, Z. Households' willingness to pay for green roof for mitigating heat island effects in Beijing (China). *Build. Environ.* **150**, 13–20 (2019).
7. IPCC. *Climate Change 2023: Synthesis Report. Contribution of Working Groups I, II and III to the Sixth Assessment Report of the Intergovernmental Panel on Climate Change* (IPCC, 2023).
8. Zheng, Q., Weng, Q. & Wang, K. Characterizing urban land changes of 30 global megacities using nighttime light time series stacks. *ISPRS J. Photogramm. Remote Sens.* **173**, 10–23 (2021).
9. Zou, Y. et al. Characterizing land use transition in China by accounting for the conflicts underlying land use structure and function. *J. Environ. Manage.* **349**, 119311 (2024).
10. Zhu, Z. et al. Understanding an urbanizing planet: Strategic directions for remote sensing. *Remote Sens. Environ.* **228**, 164–182 (2019).
11. Yu, H., Yu, L., Zhang, C. & Qi, Y. How does urbanization process affect urban heat island effect? Interpretation of 31 cities in China based on local climate zones. *Environ. Res. Lett.* **20**(11), 114013. https://doi.org/10.1088/1748-9326/ae0da5 (2025).
12. Li, T. et al. The mitigating effects of urban resilience on surface urban heat islands: Nonlinear responses, threshold effects, and spatial heterogeneity. *Sustain. Cities Soc.* **131**, 106722. https://doi.org/10.1016/j.scs.2025.106722 (2025).
13. Joshi, S. & Suneja, M. Assessing the impact of land use/land cover change on land surface temperatures and SUHI: Case of Pune, India. *Eur. J. Sustain. Dev.* **13**(3), 195. https://doi.org/10.14207/ejsd.2024.v13n3p195 (2024).
14. Li, Y. L. et al. Seasonal variation of land surface temperature and the spatial heterogeneity of its driving factors in Beijing. *J. Cap. Norm. Univ. (Nat. Sci. Eds).* **44**(5), 69–79 (2023).
15. Beijing Leading Group Office for the Third National Land Survey, Beijing Municipal Commission of Planning and Natural Resources, & Beijing Municipal Bureau of Statistics. Main data bulletin of Beijing's third national land survey. Available from: http://ghzrzyw.beijing.gov.cn/zhengwuxinxi/sjtj/tdbgdctj/202111/t20211105_2529986.html [Accessed 8th August 2024] (2021).
16. You, M., Lai, R., Lin, J. & Zhu, Z. Quantitative analysis of a spatial distribution and driving factors of the urban heat island effect: A case study of Fuzhou Central Area, China. *Int. J. Environ. Res. Public Health* **18**(24), 13088. https://doi.org/10.3390/ijerph182413088 (2021).
17. Chen, B., Xu, B. & Gong, P. Mapping essential urban land use categories (EULUC) using geospatial big data: Progress, challenges, and opportunities. *Big Earth Data* **5**(3), 410–441 (2021).
18. Allan, A. et al. Driving forces behind land use and land cover change: A systematic and bibliometric review. *Land* **11**(8), 1222 (2022).
19. Tan, Y., Xu, H. & Zhang, X. Sustainable urbanization in China: A comprehensive literature review. *Cities* **55**, 82–93 (2016).
20. Srivastava, V. T., Sharma, A. & Jadon, S. S. A review of the formation, mitigation strategies from 50 years of global urban heat island studies. *Environ. Dev. Sustain.* https://doi.org/10.1007/s10668-024-04966-y (2024).
21. Tian, L. et al. Review on urban heat island in China: Methods, its impact on buildings energy demand and mitigation strategies. *Sustainability* **13**(2), 762 (2021).
22. Liu, B. et al. Classification schemes and identification methods for urban functional zone: A review of recent papers. *Appl. Sci. (Basel)* **11**(21), 9968 (2021).
23. d Morais, M. V. B. et al. Sensitivity of radiative and thermal properties of building material in the urban atmosphere. *Sustainability* **11**, 6865 (2019).
24. Qiao, Z. et al. Spatio-temporal pattern and evolution of the urban thermal landscape in metropolitan Beijing between 2003 and 2017. *Acta Geogr. Sin.* **74**(3), 475–489 (2019).
25. Aghazadeh, F. et al. Assessing land use changes effect on urban green spaces and built-up areas summer cooling capacity. *Int. J. Environ. Sci. Technol.* **23**(2), 158. https://doi.org/10.1007/s13762-025-06968-3 (2026).

26. Beijing Municipal Forestry and Parks Bureau. Expert assessment of forest climate regulation effects in Beijing. The Paper. Available at: https://m.thepaper.cn/baijiahao_15944081 [Accessed 18th February 2026] (2021).
27. Beijing Municipal Government Implementation plan for promoting ecological protection and green development in the ecological conservation zone in the new era. Available at: https://www.beijing.gov.cn/zhengce/zhengcefagui/202301/t20230106_2892787.html [Accessed 18th February 2026] (2023).
28. Liu, Z., Yuan, H. & Luo, J. Exploring the effects of street canyon morphology on LST within different street types using causal inference and machine learning. *Sustain. Cities Soc.* **132**, 106814. https://doi.org/10.1016/j.scs.2025.106814 (2025).
29. Su, B. et al. Differences in diurnal hourly variation characteristics of surface and canopy urban heat islands in major provincial capitals of China. *Natl. Remote Sens. Bull.* **28**(8), 1885–1898 (2024).
30. Vujovic, S., Haddad, B., Karaky, H., Sebaibi, N. & Boutouil, M. Urban heat island: Causes, consequences, and mitigation measures with emphasis on reflective and permeable pavements. *CivilEng* **2**(2), 459–484. https://doi.org/10.3390/civileng2020026 (2021).
31. Beijing Municipal Commission of Development and Reform. Media report on Beijing's "Shujie Zhengzhi Cujin Tisheng" campaign and non-capital function relief. Available at: https://fgw.beijing.gov.cn/gzdt/fgzs/mtbdx/bzwlxw/202207/t20220728_2781000.htm [Accessed 18th February 2026] (2022).
32. Li, Y., Zhou, D., Yan, Z., et al. Contribution of urbanization to local warming in major cities of China. *Environ. Sci.* **43**(5), 2822–2830. https://doi.org/10.13227/j.hjkx.202109081 (2022).
33. Xu, W., Yang, H., Zhang, S., et al. Variation characteristics of urban heat island in Shanghai. J. Trop. Meteorol. 34(2), 228–238. https://doi.org/10.16032/j.issn.1004-4965.2018.02.009 (2018).
34. Ni, X. et al. Projections of urban heat island effects under future climate scenarios: A case study in Zhengzhou, China. *Remote Sens.* **17**(15), 2660 (2025).


## Author contributions

H. W. and A. G. conceptualized the study, designed the framework and drafted the manuscript. A. G., J. W and J. Z. supervised the research, revised the manuscript critically and handled correspondence. Z. F. and M. J collected and analyzed the data. All authors reviewed and approved the final manuscript.

## Declarations

## Competing interests

The authors declare no competing interests.

## Additional information

**Correspondence** and requests for materials should be addressed to A.G.

**Reprints and permissions information** is available at www.nature.com/reprints.

**Publisher's note** Springer Nature remains neutral with regard to jurisdictional claims in published maps and institutional affiliations.